STScI | SPACE TELESCOPE SCIENCE INSTITUTE

Instrument Science Report WFC3 2017-08

Monitoring the WFC3/UVIS Relative Gain with Internal Flatfields

J. Fowler & S. Baggett

March 15, 2017

Abstract

The WFC3/UVIS gain stability has been monitored twice yearly. This project provides a new examination of gain stability, making use of the existing internal flatfield observations taken every three days (for the Bowtie monitor) for a regular look at relative gain stability. Amplifiers are examined for consistency both in comparison to each other and over time, by normalizing the B, C, and D amplifiers to A, and then plotting statistics for each of the three normalized amplifiers with time. We find minimal trends in these statistics, with a $\sim 0.02 - 0.2\%$ *change in mean amplifier ratio over 7.5 years. The trends in the amplifiers are well-behaved with the exception of the B/A ratio, which shows increased scatter in mean, median, and standard deviation. The cause of the scatter remains unclear though we find it is not dependent upon detector defects, filter features, or shutter effects, and is only observable after pixel flagging (both from the data quality arrays and outlier values) has been applied.*

Introduction

The Hubble Wide Field Camera 3 (WFC3) UVIS channel is split into two chips (Chip 1 and 2) and four amplifiers (A, B, C, and D). Each amplifier has a corresponding gain calibration correction (nominal value stored in the FITS header) which converts the digital counts recorded in each amp to electrons.

Past gain monitoring has been done by measuring the absolute gain values of the four amplifiers using the standard mean-variance technique and to date, the values have been stable to 1-2% (e.g. Martlin, 2016). A crucial assessment, such a technique does require considerable observing time in order to collect a sufficient number of flatfields at a range of different exposure levels and thus, the absolute gain check is only performed twice per year. Relative gain measurements, where one quadrant of the image is used as a fiducial for the other three, can be performed on single images taken with the same observing setup. Assuming the light source and illumination pattern across the field of view are stable, such a measure provides insight into the stability of the relative amplifier gains. While the relative gains cannot be used directly to convert counts to electrons, they can serve as a useful monitor of the health and stability of the instrument.

Observations

The Bowtie observing program began immediately after WFC3 was installed into HST, to monitor and correct for quantum efficiency hysteresis which may arise (Baggett & Borders, 2009). The program has worked very well over the years with the monitoring now entirely automated and the data fairly stable (Bourque & Baggett, 2013). The calibration images necessary for the Bowtie monitor are UVIS internal tungsten flatfield exposures currently collected every 3 days. They make use of the 3x3 binned subarray observing mode to optimize observing efficiency. The image format for Bowtie observations is shown in Figure 1, and the Bowtie monitor proposals are shown in Table 1.

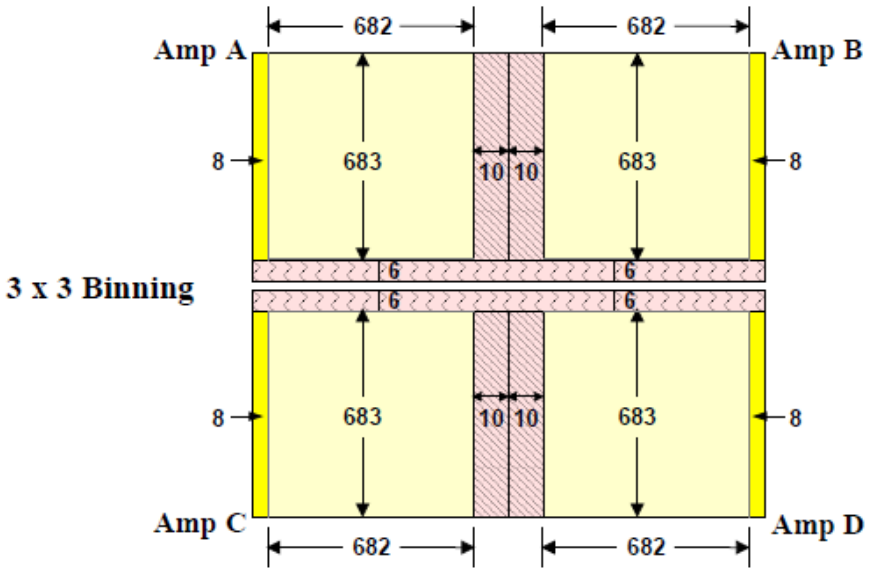

Fig. 1.—*Image format for WFC3/UVIS. The detection area of the 4 amplifiers is represented by the pale yellow area of the diagram. Courtesy of the WFC3 Instrument Handbook (Dressel, 2017).*

Program ID	Program Title	PI	Cycle
11808	UVIS Bowtie Monitor	J. MacKenty	SMOV
11907	UVIS Bowtie Monitor	S. Baggett	17
12344	UVIS Bowtie Monitor	T. Borders	18
12688	UVIS Bowtie Monitor	T. Borders	19
13072	UVIS Bowtie Monitor	M. Bourque	20
13555	UVIS Bowtie Monitor	M. Bourque	21
14001	UVIS Bowtie Monitor	M. Durbin	22
14367	UVIS Bowtie Monitor	M. Durbin	23
14530	UVIS Bowtie Monitor	B. Sunnquist	24

Table 1:*The 9 past and current cycles of Bowtie Monitor proposals. The SMOV proposal was taken during the Servicing Mission and Orbital Verification time period. In addition to those listed above, each anneal proposal also includes a 1 second Bowtie exposure after the cooldown.*

A bowtie visit consists of two 1 second unsaturated exposures sandwiching a 200 second (saturated) exposure. The F475X filter, with its high throughput and blue spectral range, is the optimum choice for negating any hysteresis effects which may develop and conditioning the detector. The high cadence and single filter usage of this program are ideal for monitoring the relative gain, though the 200 second exposures are unusable for this purpose, as they are intentionally saturated. An example of a standard unsaturated Bowtie monitor image and the ratio image created over the course of this analysis is shown in Figure 2

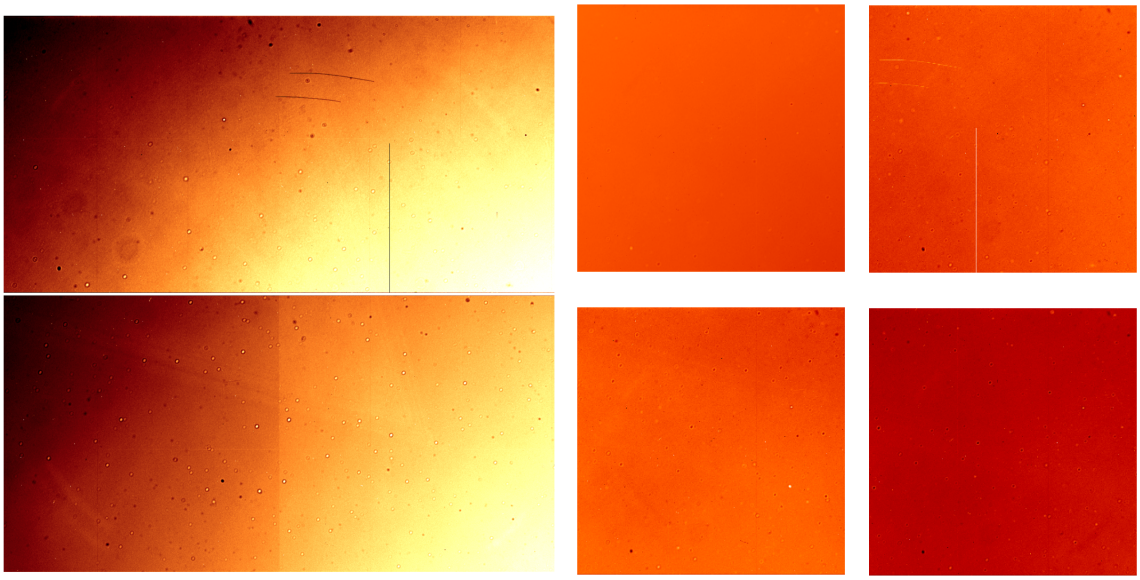

Fig. 2.—*Left: Full-frame 3x3 binned internal flatfield images that make up the Bowtie monitor data. (Top: Chip 1, Bottom: Chip 2). Right: An example of the ratio'd amplifiers (Top: A, B, Bottom: C, D). Because A is not ratio'd, it has a different scale, from 500-40000, whereas the three ratio'd amplifiers have a scale of .75-1.75.*

Data Collection and Quality

This project began by collecting archival data from the internal-only WFC3 Quicklook database (Bourque et al., 2016). Bowtie monitor images are selected out with `Python` queries to Quicklook, querying for tungsten UVIS flats with the F475X filter, and binned 3 by 3, as well as the aforementioned further selection of 1 second unsaturated exposures. The specifics of querying the Quicklook database are provided in Appendix A.

Every image – bowtie or otherwise – is prone to detector effects that create increased or decreased pixel values not reflective of the object or conditions of the image. Some of this is obviously visible, for example the vertical pixel line (bad data column) and the two curved scratches in the B quadrant shown in Figure 2.

Every image comes with an associated Data Quality (DQ) array with non-zero values for any issue per pixel, ranging from a bad detector pixel to a pixel affected by an anomaly, etc. Table 2 lists the flags (and their associated error or anomaly type) that may be present in a DQ array. The first set of applied flagging consisted of ignoring any pixel marked in the DQ array, i.e. flagging all but the `DQ == 0` values. This can flag $\sim$ 11000 pixels – the exact number will vary with each image.

Flag Value	Data Quality Condition (UVIS)
0	No Error
1	Reed-Solomon decoding error
2	Data replaced by fill value
4	Bad detector pixel
8	unused flag for UVIS
16	Hot pixel
32	CTE tail
64	Warm pixel
128	Bad pixel in bias
256	Full-well saturation
512	Bad or uncertain flat value
1024	Charge trap
2048	A-to-D saturation
4096	Cosmic ray detected by AstroDrizzle
8192	Cosmic ray detected by CR-SPLIT or REPEAT-OBS
16384	Pixel affected by ghost or crosstalk (unused)

Table 2:*The Data Quality flags (for cycle 24) of WFC3/UVIS (Dressel, 2017). The flags are bitwise, so multiple flags can be included for a single pixel. Our flagging removes any pixel with a non-zero DQ flag.*

However for completeness outlier pixels were also flagged after the DQ flagging. For each of the three amplifier images normalized to amp A, 4000 of the outlier pixels (2000 of

the highest and 2000 of the lowest, about $\sim 0.5\%$ total of the image) were excluded from the statistics. This in turn removes 12000 more pixels from the image, meaning in total as much as $\sim 1\%$ of any given image may be flagged. Figure 3 shows the three normalized amplifiers with their non-zero DQ and minimum and maximum pixels marked.

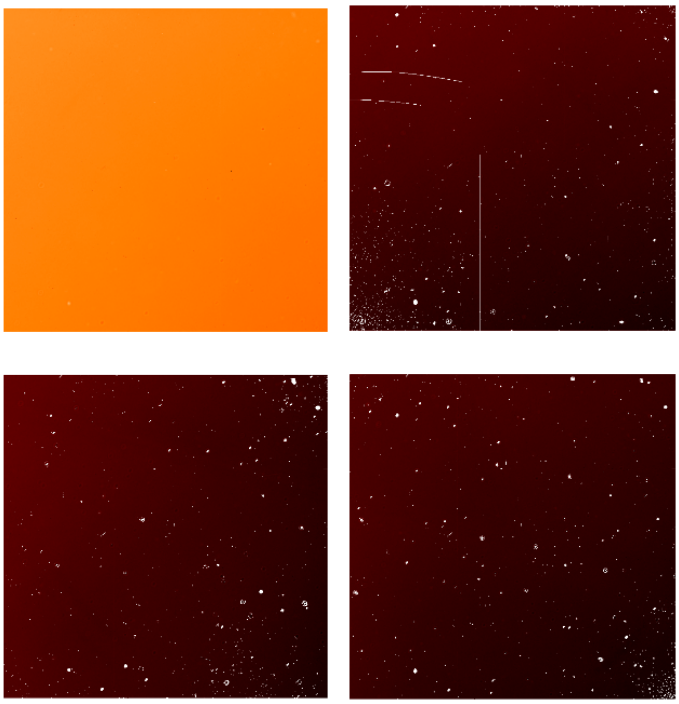

Fig. 3.—*Amplifier A and ratios B (top) and C and D (bottom). The flagged non-zero DQ pixels as well as minimum and maximum values are in white. A is left untouched as it is not ratio'd or flagged.*

The final statistics taken were clipped using the `sigmaclip` function in `Scipy`, and the mean, median, standard deviation, minimum, and maximum for each image was calculated. The `sigmaclip` was set with a lower and upper bound of 2, meaning that the function will iteratively remove values until all points are bounded within 2σ on either side of the data. These final statistics, along with the days elapsed since the Bowtie monitor data collection began (June 11th, 2009) and the file name and location within the WFC3 database were written to a running table that is presently part of an automated monitor for relative amplifier gain. There are presently ~ 2400 of these images (and more every three days), and an abridged sample of the table is shown in Table 3.

Results

Having collected statistics, figures like Figure 5 were produced. However, some hysteresis is introduced through monthly anneals. As part of the regular monthly anneal procedures performed to fix hot pixels, the WFC3/UVIS detector is warmed up then cooled back down.

root name	mean B	med B	std B	max B	min B	time
ibc183qjq	1.108	1.108	0.018	1.144	1.072	294
ibct4wa1q	1.111	1.110	0.017	1.146	1.075	479
ibct2crrq	1.111	1.110	0.017	1.147	1.075	336
ibct01acq	1.111	1.110	0.018	1.147	1.075	60
ibct4wzyq	1.111	1.111	0.018	1.148	1.075	479

Table 3:*Sample of statistics collected from Bowtie monitor images of just a few dates and a single amplifier. We calculated the statistics for the three ratio'd amplifiers, B, C, and D to A, and the time is recorded in units of days elapsed since Bowtie monitor data began.*

This process results in a low-level hysteresis (Bourque & Baggett, 2013) which affects the level and illumination pattern of (only) the first internal flatfield taken after the anneal. For completeness, we leave the hysteresis affected data in these figures but omit them from the fits. The hysteresis cutoffs applied for the fits are shown in Figure 4 as well as enumerated in Table 4. Hysteresis will present in the same images regardless of amplifier, but applying hysteresis cut offs individually across the 3 amplifiers provided a consistency check, as well as an easy way to apply other cut offs (which became relevant in examining Amp B's increased scatter.) For each amplifier $\sim$ 100 points were flagged; there were 93 points (or images) in common flagged for the three ratio'd amplifiers, and $>$ 97% of those matched anneal dates (when we expect to see hysteresis.) Hysteresis images could of course be identified manually but the intent of using the measured statistics to perform the flagging is to enable automation of the relative gain monitor.

Amplifier	Cutoff Set	Condition
B	minimum	> 1.0739
C	mean	> 1.084
D	median	< 1.26

Table 4:*The above criteria were chosen from visual inspection of the initial data to identify hysteresis. Points that did not meet the cutoff condition were flagged as hysteresis, and these points were omitted from fit calculations for all statistics on that amplifier.*

Plotting each statistic reveals that there is little change in the instrument with time or across amplifier. The mean and median are shown in Figures 5 and 6. The mean and median for B/A and C/A are extremely flat with $< 0.05\%$ total change over the last 7.5 years. However D/A shows a slight trend upwards with time, about 0.2% over the 7.5 years in orbit. Although small, the trend is some 5-10 times that seen in the B/A and C/A ratios and will require continued monitoring. For completeness, we also check the relative gain using other amplifiers as the comparison (see Appendix C). Those plots similarly indicate that amplifier D may be changing very slowly over time, e.g., the trend seen in D/A is inversely imprinted on the B/D and C/D ratios (as well as of course the A/D ratio, as shown in Figures 19 and 20).

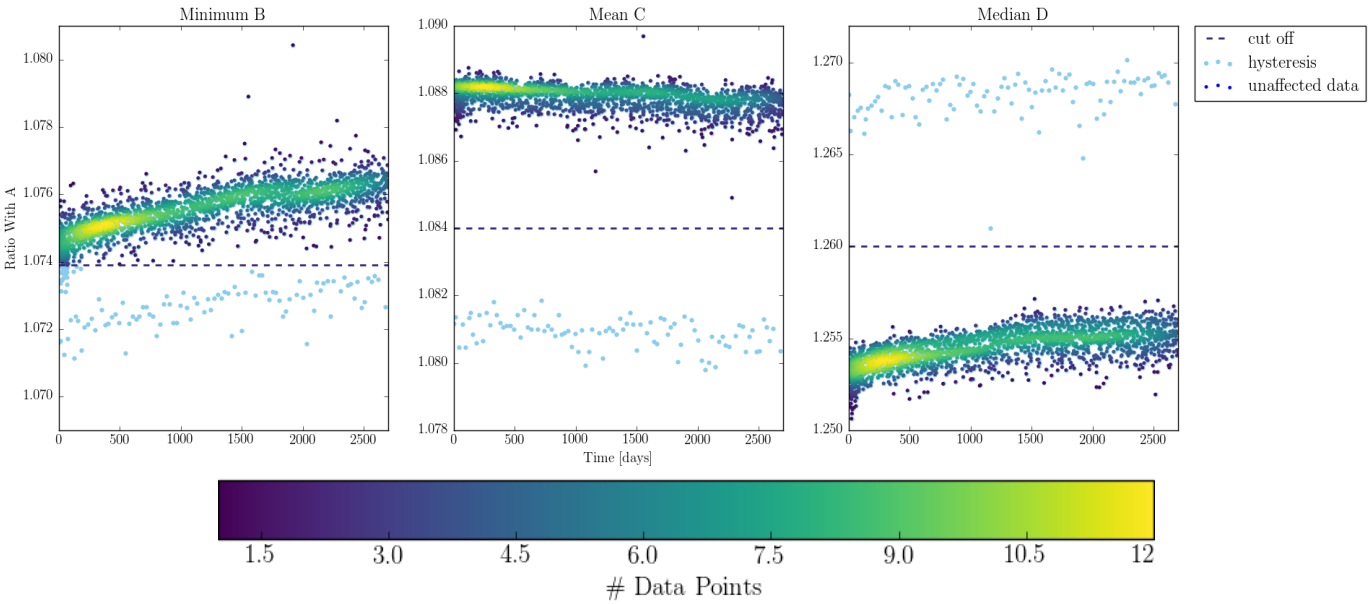

Fig. 4.—*These three statistics were chosen as the most clear examples of hysteresis for each amplifier. While hysteresis will affect images as a whole and be echoed in all statstics and all amplifiers, flagging the three amplifiers individually allows a check for consistency. The colormap represents point densities, and the above scale is consistent for all density map plots within this report.*

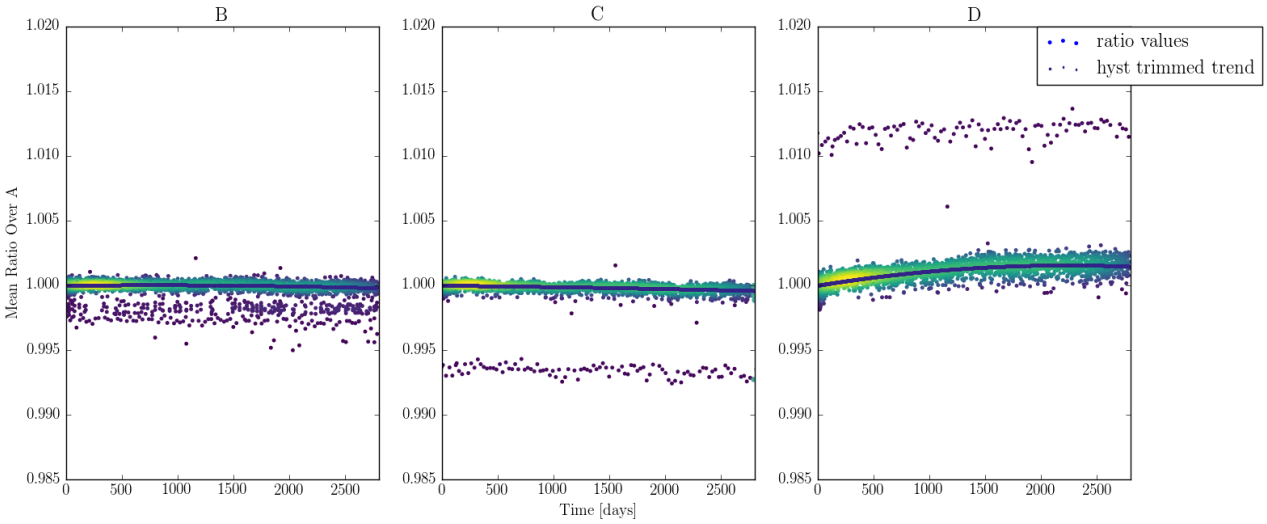

Fig. 5.—*Mean gain for each amplifier relative to amp A as a function of day since June 11th, 2009. The plotted data were normalized to display a percent difference. Points are plotted with the density map in Figure 4. The blue fit curve was calculated omitting the points flagged as impacted by hysteresis and the increased scatter in B (discussed in detail in the next section.)*

The additional collected statistics – standard deviation, maximum, and minimum, are shown in Appendix B.

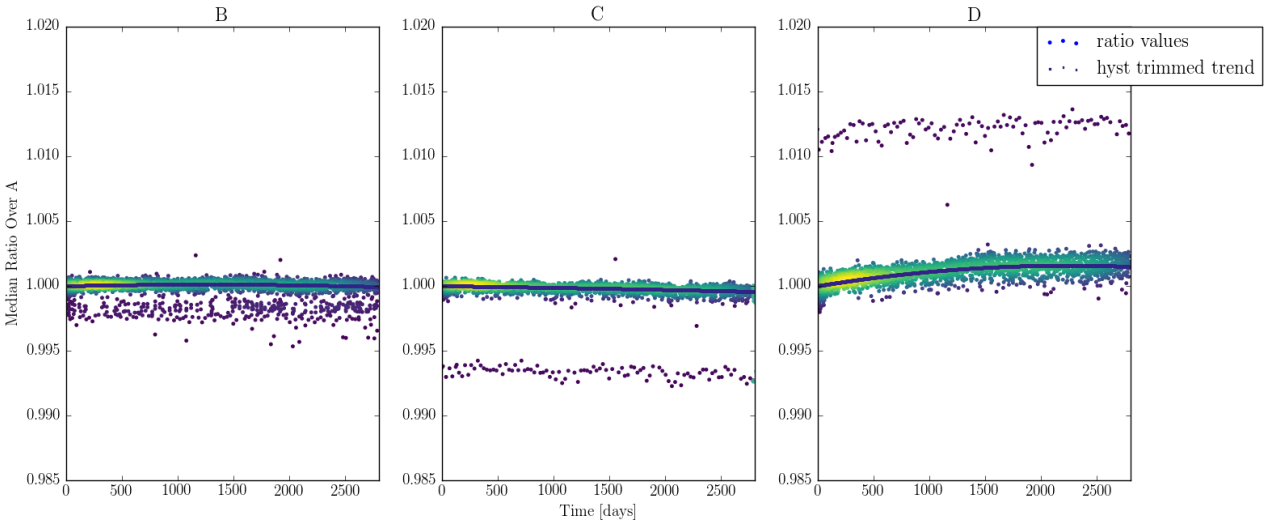

Fig. 6.—*Median gain for each amplifier as a function of day since June 11th, 2009.*

Increased Scatter in Amp B

We note that the mean and median for B/A show more scatter than the mean and median for C/A and D/A. Despite the same images making up hysteresis in each amplifier, Amp B shows an intermediary population of scatter between the main trend and hysteresis affected imges. As shown in Figure 7, some of the outlier points in B/A are due to hysteresis images but others are nominal internal flatfields.

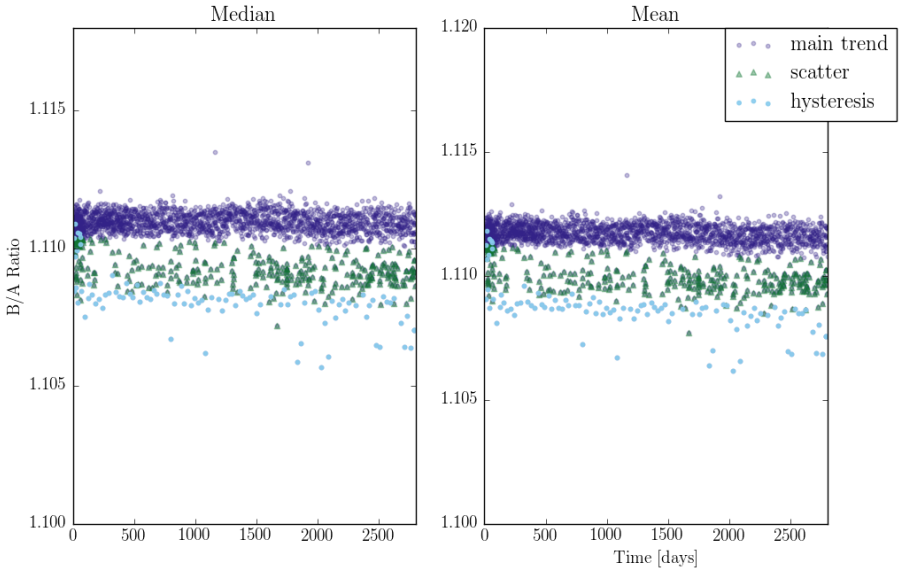

Fig. 7.—*Left: Median ratio. Right: Mean ratio. The hysteresis makes up a small portion of the scatter points below the main trend.*

We investigated many potential sources for the increased scatter, including scatter due to one of the shutters, some peculiarity in the flagging, and filter effects that only present themselves for ratios of ratio'd amplifiers. The scatter appears only after flagging is applied.

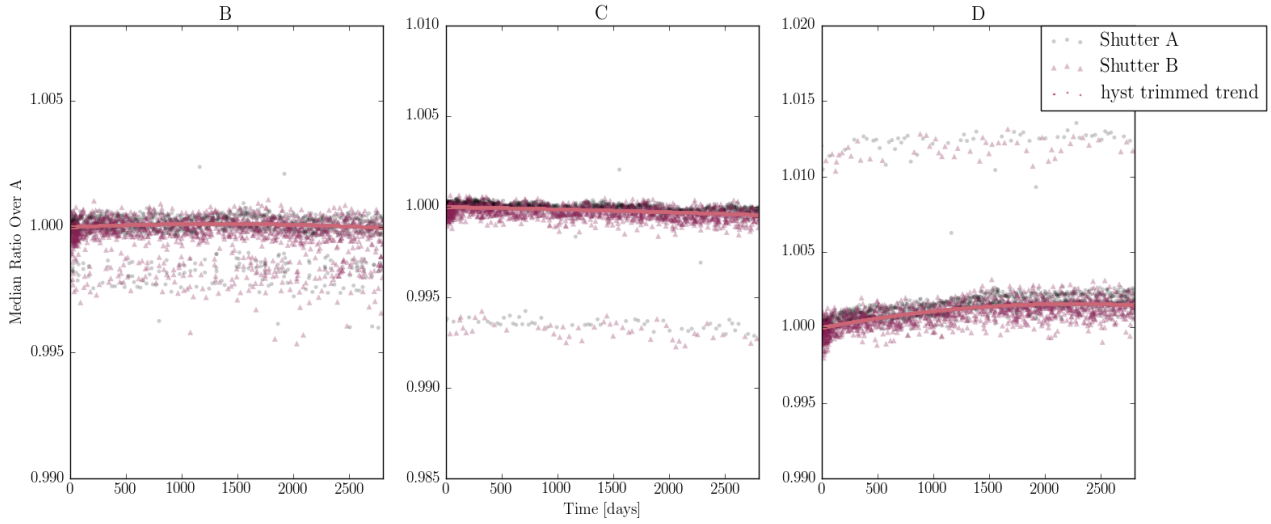

Fig. 8.—*Median amplifier ratios split by shutter. Notice that the images taken in either shutter make up the scatter areas of amp B, and make up fairly similar populations in amp C and D, though Shutter B presents systematically lower within the main trend.*

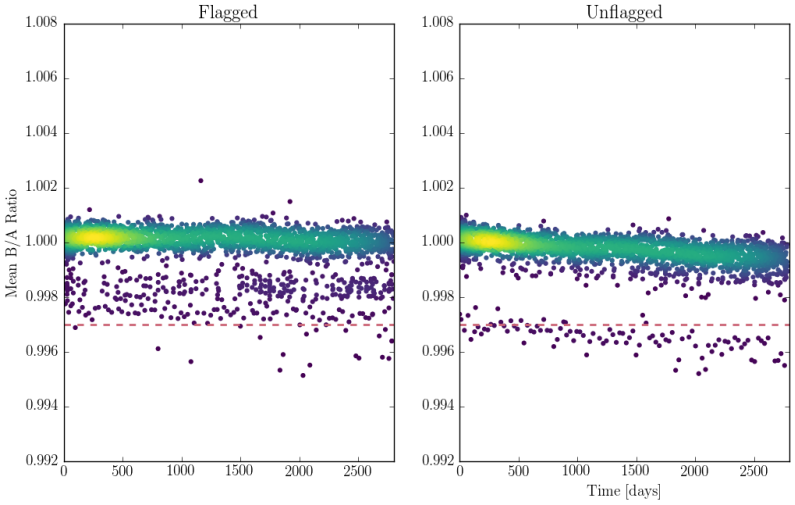

Fig. 9.—*Left: Flagged mean B ratio. Right: Unflagged mean B ratio. It appears as if the scatter vanishes from amp B when plotted with unflagged statistics. The cause of this is unclear. The dotted line indicates the increased percent difference between the main trend and the hysteresis points in the unflagged mean of amplifier B.*

First, we test whether the scatter points are preferentially from one shutter or another. In examining the difference in shutter A and shutter B for the 3 amplifiers, while we found

some subtle variation in the main trend, we found no notable difference in the distribution of the scatter, as shown in Figure 8.

In the next test, we investigate the impact of flagging bad pixels. The obvious bad column and two scratches which fall in the B quadrant (visible in Figures 2 and 3) are masked before statistics are measured. We examined the comparison on the flagged and unflagged statistics, as shown in Figure 9. The unflagged statistics for amp B appear to eliminate the scatter and a careful examination of the scale shows that the unflagged statistics have a much greater standard deviation from the general trend line.

Another test, meant to examine subtle differences in the high and low images within the amplifier was comparing an A/B ratio for a high registering point to an A/B ratio for a low registering point, an example of which is shown in Figure 10. Many of these images showed evidence of a 'droplet', a common effect when the F475X filter wheel does not return to precisely the same position (Bourque & Baggett, 2013). However, in the tested ratio of ratios, this was just as common in the C and D ratios as amplifier B, and therefore would not add to the increased scatter seen only in B.

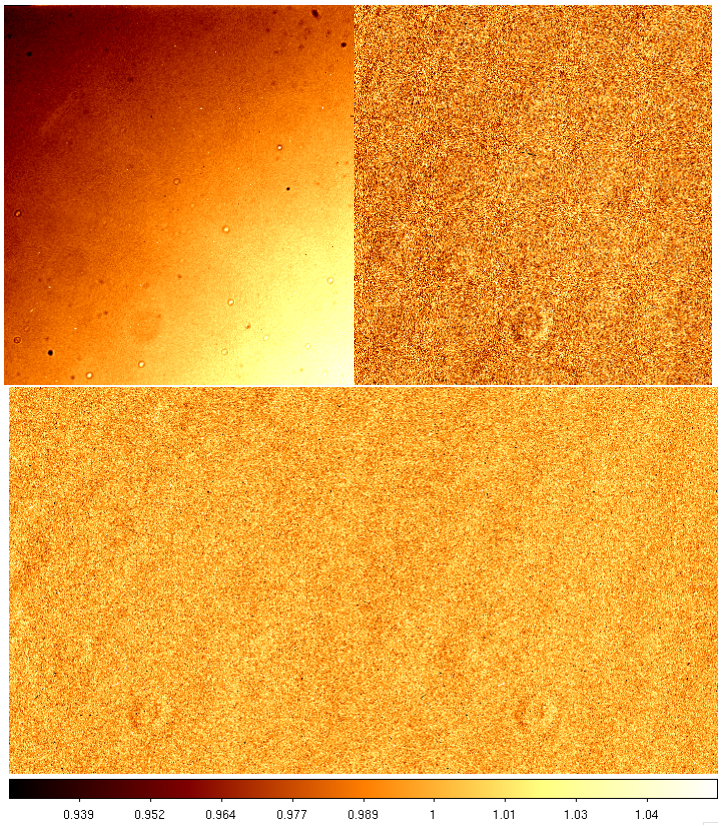

Fig. 10.—*These double ratio images compare the normalized amplifiers for high and low registering data points. The droplet effect appears in all three amplifiers. Top Left: Unaltered A, as it is never ratio'd. Top Right: Amp B. Bottom Left: Amp C. Bottom Right: Amp D. The scale at the bottom applies to all amplifier ratios, but not amp A.*

Fit Curves and Total Amplifier Change

Each set of data was also fit with a two-dimensional curve using `numpy.polyfit` in `Python`, as well as a line a best fit to estimate the total amplifier change. Both fits excluded the points affected by hysteresis, and in the case of amplifier B the fits were calculated without hysteresis and without the extra scatter, simply by applying a cut off that excluded the scatter and hysteresis in the data. A brief numerical analysis of two-dimensional (and for completeness four-dimensional) curves in `Mathematica` showed no obvious discontinuity or local maxima of interest in the fits. The slopes of each one-dimensional fit line are shown in Table 5. The slopes of the ratio of each statistic are on the order of 10^{-7} per day at most (i.e., of the order $\sim 0.05\%$ over 7.5 years).

Amp	Mean	Med	Std	Max	Min
B	-6.41×10^{-8}	-4.33×10^{-9}	-3.66×10^{-7}	-7.97×10^{-7}	6.68×10^{-7}
C	-1.55×10^{-7}	-1.67×10^{-7}	1.49×10^{-7}	1.43×10^{-7}	-4.52×10^{-7}
D	7.34×10^{-7}	7.46×10^{-7}	-1.51×10^{-7}	4.31×10^{-7}	1.04×10^{-6}

Table 5: *The slope of each statistic, in ratio with amplifier A per day.*

The amplifier ratios, as measured from the frequent flatfields taken for the Bowtie monitor, have been extremely stable over the past 7.5 years. The total change in the means of the ratio over the ~ 7.5 years has been $\sim 0.02\%$, $\sim 0.04\%$, and 0.2% for B/A, C/A, and D/A. The absolute gain ratios have remained constant to within $1-2\%$ over the same time period (Martlin, 2016).

Acknowledgements

A special thanks to Matthew Bourque and his endless patience helping me understand Quicklook, Catherine Martlin for her assistance with creating interactive and automated monitors, and Gabe Brammer for reviewing and providing feedback for this ISR.

REFERENCES

ISR 2009-24: WFC3 SMOV Proposal 11808: UVIS Bowtie Monitor, S. Baggett & T. Borders 26 Jan 2010

ISR 2013-09: WFC3/UVIS Bowtie Monitor, M. Bourque & S. Baggett 25 Jun 2013

Dressel, L. 2017, "Wide Field Camera 3 Instrument Handbook, Version 9.0" (Baltimore: STScI)

ISR 2016-13: WFC3 Cycle 23 Proposal 14373: UVIS Gain, C. Martlin 03 Aug 2016

The Hubble Space Telescope Wide Field Camera 3 Quicklook Project, Bourque, Matthew, Bajaj, Varun, Bowers, Ariel, Dulude, Micheal, Durbin, Meredith, Gosmeyer, Catherine, Gunning, Heather, Khandrika, Harish, Martlin, Catherine, Sunnquist, Ben, Viana, Alex, ADASS 2016 (proceedings in press)

Appendix A

Below is some additional information about querying the internal-only WFC3 Quicklook database.

Using `pyql`, a package maintained by the WFC3 Team, the Quicklook database can be queried using `Python`. Filters allow you to sort for data specifics, including filter, target, etc from different FITS extensions of the files, and collect whichever of those properties for further use. Figure 11 shows the `Python` code required to query the Quicklook database for 1 second Bowtie exposures.

```
# quicklook imports
from pyql.database.ql_database_interface import session
from pyql.database.ql_database_interface import Master
from pyql.database.ql_database_interface import UVIS_flt_0
from pyql.database.ql_database_interface import UVIS_flt_1

def query(date):
    # Do the initial query
    results = session.query(Master.dir, Master.rootname).\
              join(UVIS_flt_0).join(UVIS_flt_1).\
              filter(UVIS_flt_0.date_obs > date,
                  UVIS_flt_0.targname == 'tungsten',
                  UVIS_flt_0.filter == 'f475x',
                  UVIS_flt_0.detector == 'uvis',
                  UVIS_flt_0.imagetyp == 'flat',
                  UVIS_flt_0.exptime == 1).\
              filter(UVIS_flt_1.binaxis1 == 3,
                  UVIS_flt_1.binaxis2 == 3).all()

    # Turn the roots and dirs into locations we can use later.
    locales = ['{}_flt.fits'.format(os.path.join(item.dir, item.rootname)) for
        item in results]

    return locales
```

Fig. 11.—Code to query the Quicklook database for 1 second Bowtie monitor images. This function in particular allows collection of Bowtie images after a certain date, which makes the process of updating a record of Bowtie monitor statistics more convenient.

Appendix B

For completeness, below are the additional statistics across the Bowtie monitor data.

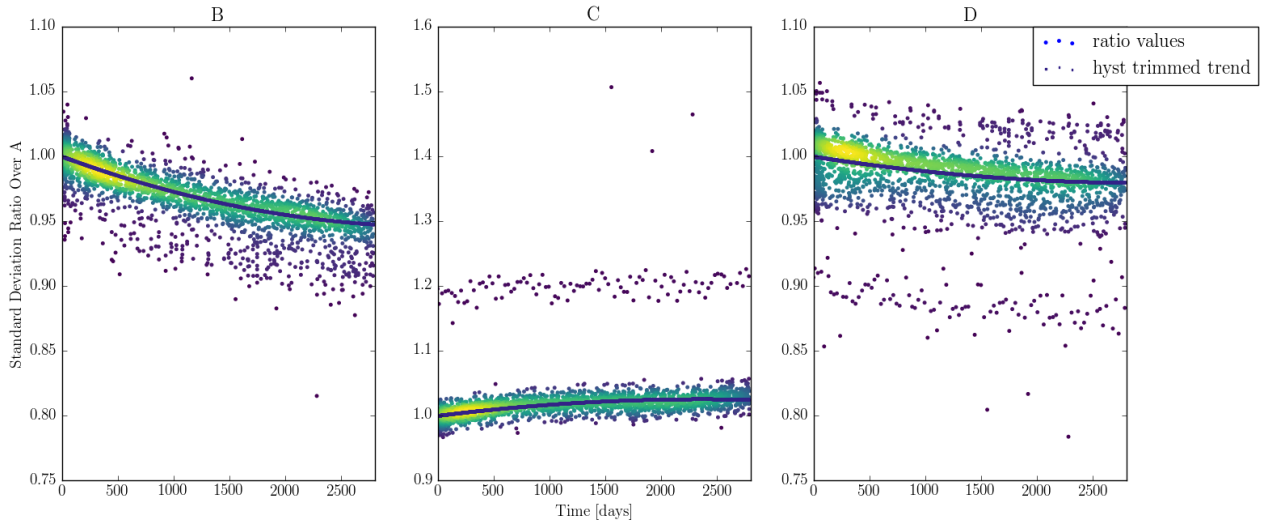

Fig. 12.—*Standard deviation of the gain ratio for each amplifier as a function of day since June 11th, 2009. Like the median and mean statistics, amplifier B lacks an obvious distinction between hysteresis affected images and nominal flatfields.*

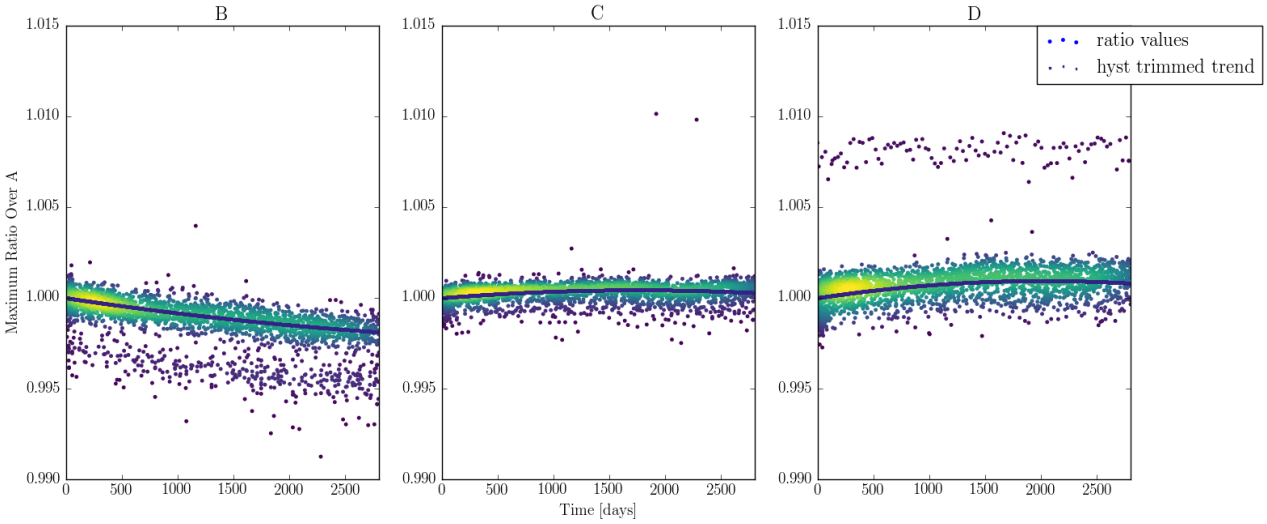

Fig. 13.—*Maximum pixel in relative gain ratio for each amplifier as a function of day since June 11th, 2009.*

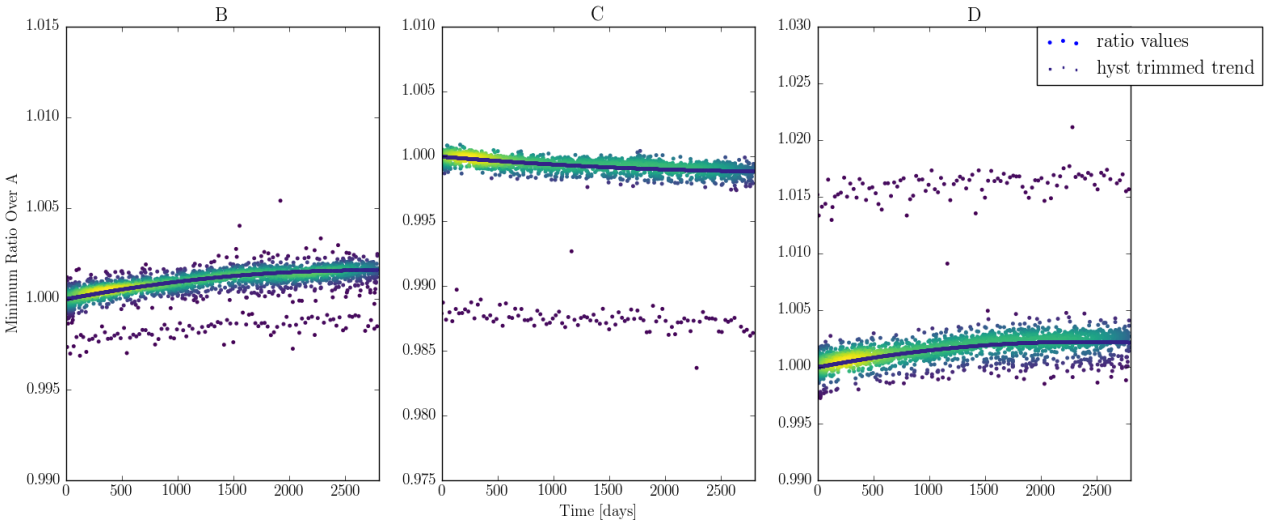

Fig. 14.—*Minimum pixel in relative gain ratio for each amplifier as a function of day since June 11th, 2009.*

Appendix C

Below are the mean and median statistics run on ratios with B, C, and D.

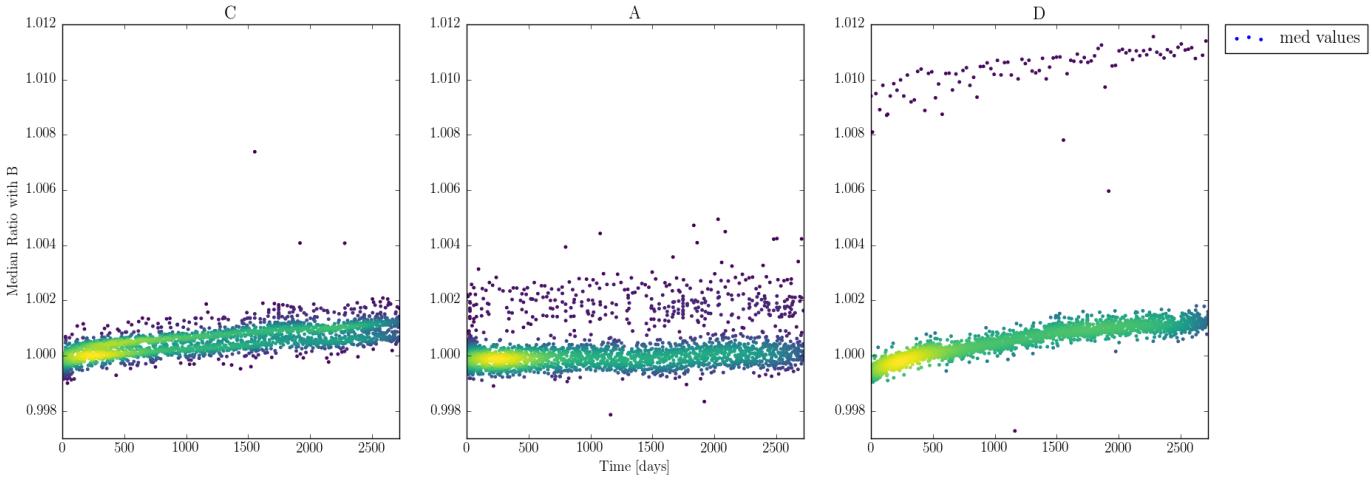

Fig. 15.—*Median of the gain ratio with respect to B for each amplifier as a function of day since June 11th, 2009.*

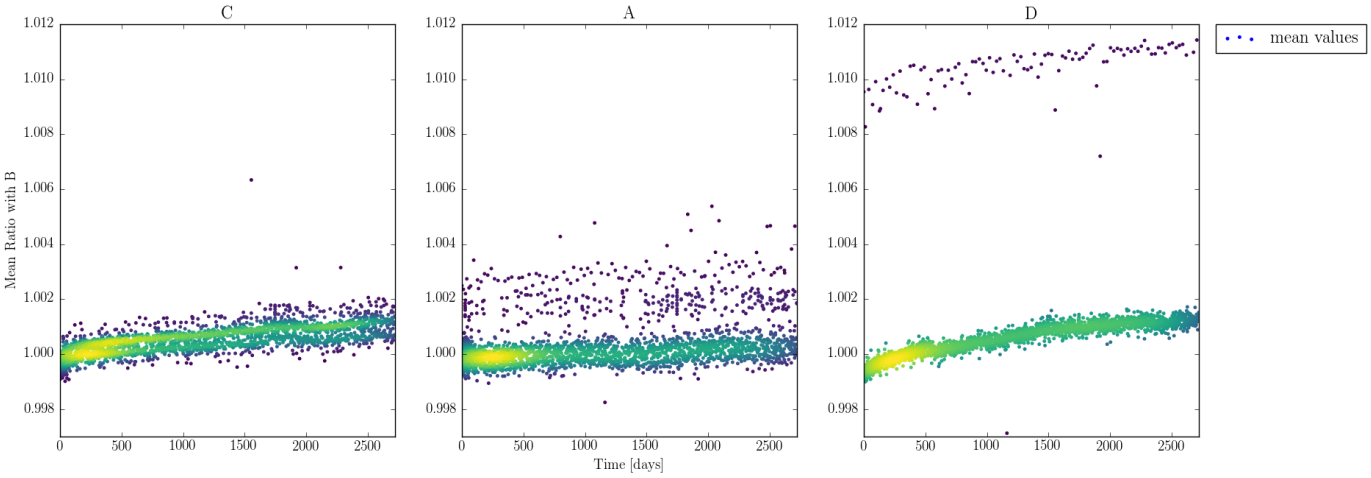

Fig. 16.—*Mean of the gain ratio with respect to B since June 11th, 2009.*

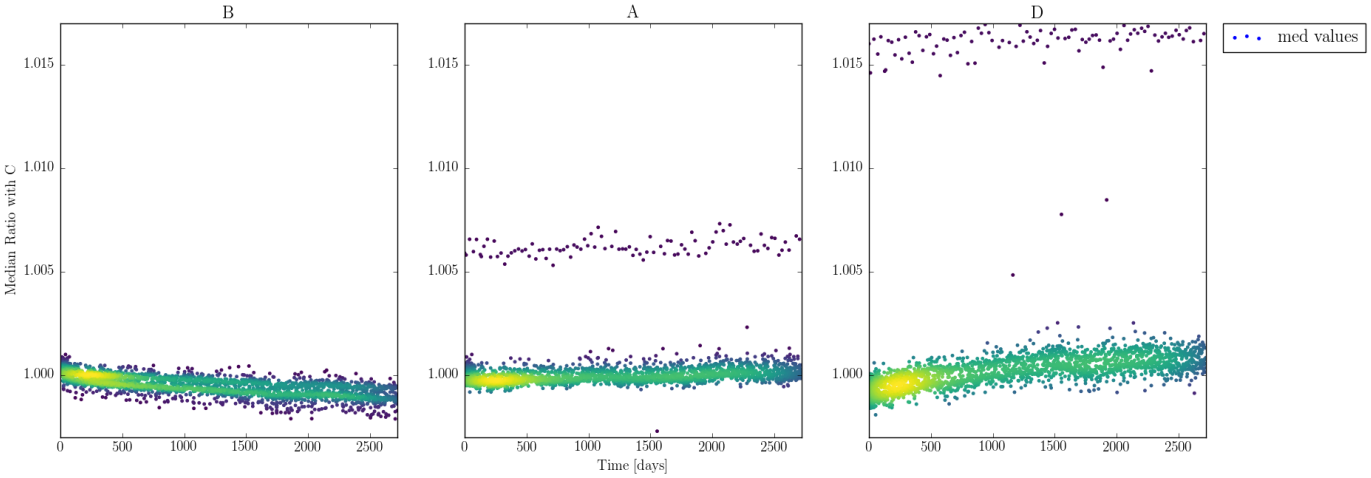

Fig. 17.—*Median of the gain ratio with respect to C since June 11th, 2009.*

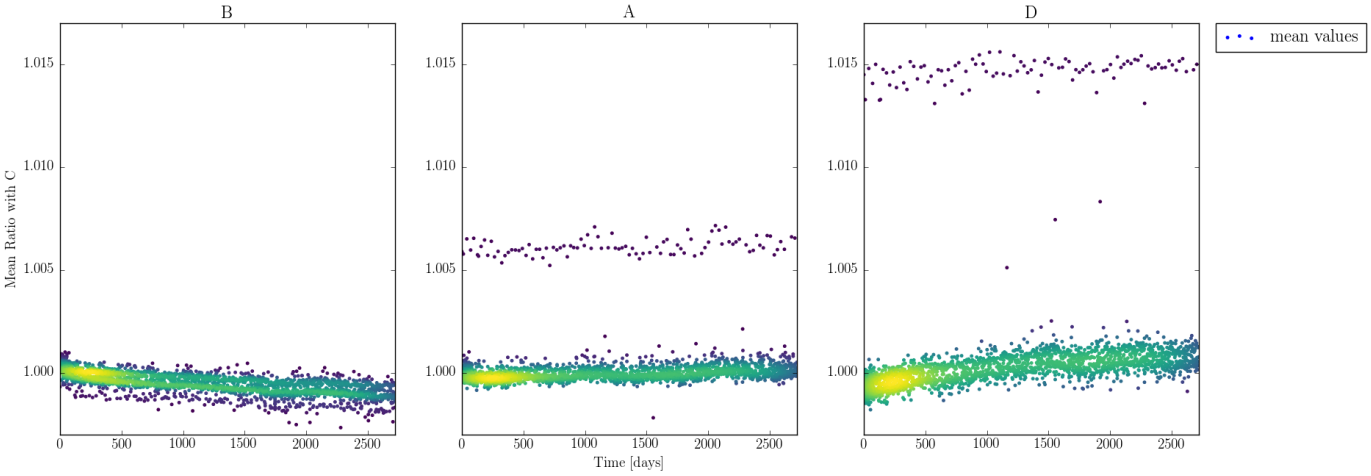

Fig. 18.—*Mean of the gain ratio with respect to C since June 11th, 2009.*

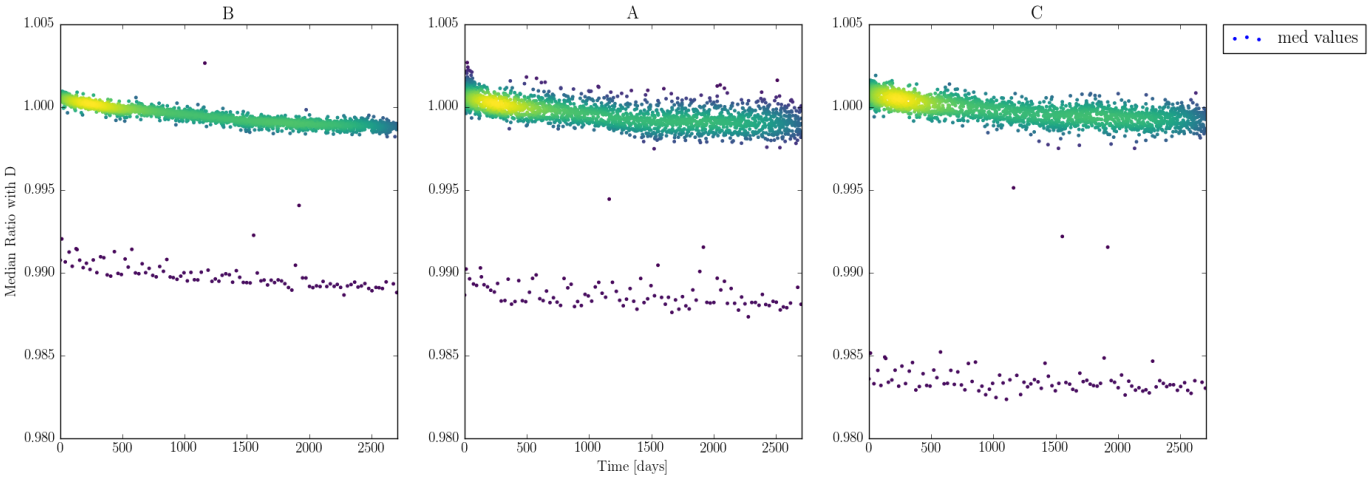

Fig. 19.—*Median of the gain ratio with respect to D since June 11th, 2009.*

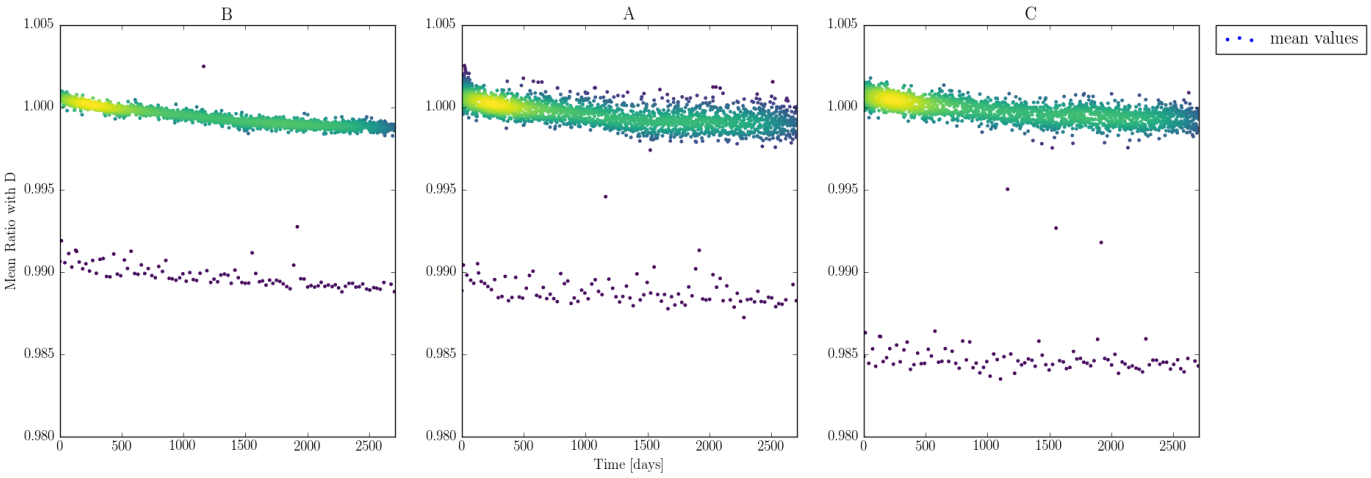

Fig. 20.—*Mean of the gain ratio with respect to D since June 11th, 2009.*